RAPID COMMUNICATIONS

PHYSICAL REVIEW A VOLUME 52, NUMBER 6 DECEMBER 1995

Direct two-color photoassociative ionization in a rubidium magneto-optic trap

D. Leonhardt and J. Weiner

Chemical Physics Program and Department of Chemistry and Biochemistry, University of Maryland, College Park, Maryland 20742

(Received 12 June 1995; revised manuscript received 11 August 1995)

We report the observation of direct, two-color photoassociative ionization (PAI) in collisions between ^{85}Rb atoms optically cooled and confined in a magneto-optical trap. We also measure the resulting Rb_2^+ ion spectrum and compare it to earlier trap-loss fluoresecence spectra. Unlike PAI in Na, which ionizes principally by collisional autoionization, the Rb_2^* intermediate photoionizes directly to Rb_2^+ in a fixed optical field. These observations confirm PAI as a sensitive and broadly applicable spectroscopic tool.

PACS number(s): 32.80.Pj, 33.80.Ps, 34.50.Rk, 34.80.Qb

The development of the magneto-optic trap (MOT) as a reaction vessel to study gas-phase bond-forming collisions in ultracold atomic samples has opened the way to rapid advances in the understanding and control of ultracold collision dynamics. Notable among these has been the study of photoassociative ionization (PAI) in sodium atom collisions. This process involves a two-step, two-photon absorption during the course of the collisional encounter. In the first step ultracold atoms approaching on a ground-state continuum absorb a photon to an excited attractive molecular state,

$$Na(^2S_{1/2}) + Na(^2S_{1/2}) + \hbar\omega_a \rightarrow Na_2^*. \quad (1)$$

The two atoms begin to accelerate toward each other, and absorb a second photon in one of two ways: (1) population of a doubly excited state while the two nuclei are relatively distant, followed by autoionization at close range (collisional PAI),

$$Na_2^* + \hbar\omega_b \rightarrow Na_2^{**} \rightarrow Na_2^+ \quad (2)$$

or (2) direct photoionization at close internuclear separation to the final molecular ion (direct PAI),

$$Na_2^* + \hbar\omega_b \rightarrow Na_2^+. \quad (3)$$

Figure 1(a) diagrams these two possibilities. Over the detuning range of $\hbar\omega_a$ where the collisional channel is open [~ 17 cm^{-1} from the $Na(^2P_{3/2}) + Na(^2S_{1/2})$ dissociation limit], collisional PAI dominates by a factor of over 10^7 [1]. Delineation of high-resolution spectroscopy and optical control of PAI in sodium has advanced rapidly over the past few years and remains an active area of research [2–4].

Figure 1(b) shows the analogous potential curves and transitions on rubidium molecular potentials. In contrast to sodium the asymptote of the doubly excited levels lies 1700 cm^{-1} below the Rb_2^+ potential minimum; and therefore, at ultracold temperatures, the channel for collisional PAI is closed. The molecular ion can only be formed by direct photoionization of the Rb_2^* collisional intermediate, all the way to the dissociation limit. The two-step PAI process in rubidium is therefore

$$Rb(^2S_{1/2}) + Rb(^2S_{1/2}) + \hbar\omega_p \rightarrow Rb_2^* \quad (4)$$

followed by

$$Rb_2^* + \hbar\omega_t \rightarrow Rb_2^+ + e, \quad (5)$$

where ω_p denotes probe laser frequency and ω_t denotes transfer or ionization laser frequency. By sweeping $\hbar\omega_p$ as far as 35 GHz to the red of the $Rb(^2P_{3/2}) + Rb(^2S_{1/2})$ dissociation limit, we have generated a direct PAI spectrum arising from free-bound transitions to molecular states in the first step of the PAI process. We emphasize that this direct, two-color PAI spectrum does not depend on the presence of open autoionizing channels and establishes PAI as a generally applicable spectroscopic technique. Virtually *any* two ultracold colliding partners should exhibit a direct, two-color PAI spectrum.

The heart of the apparatus is a magneto-optic trap loaded from residual ^{85}Rb background gas. Figure 2 shows a schematic of the experimental setup. The vapor cell (MOT) [5,6] is formed in a stainless steel vacuum chamber with a back-

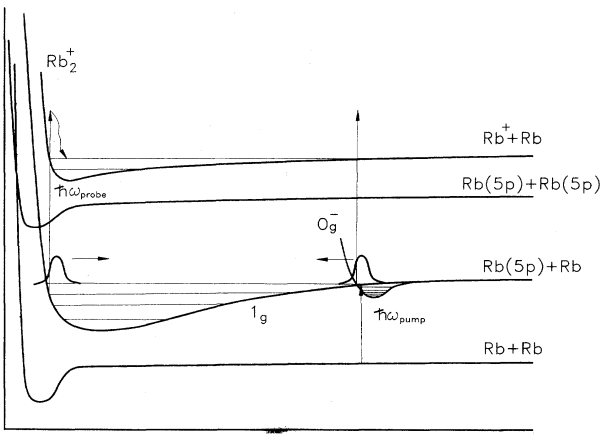

FIG. 1. (a) Schematic potentials and transitions relevant to PAI in sodium. Note that there are two pathways to PAI: (1) Optical coupling to an attractive excited state followed by a second optical transition to a doubly excited state. The doubly excited state then undergoes autoionization at short range to produce the final $Na_2^+ + e$ product (dashed arrows). (2) Optical coupling to an attractive excited state followed by photoionization directly to $Na_2^+ + e$ (solid arrows). (b) Analogous potentials and transitions in ^{85}Rb collisions. Note that the energy gap between the doubly excited asymptote and the minimum of the molecular ion potential closes the autoionization channel at ultracold temperatures.

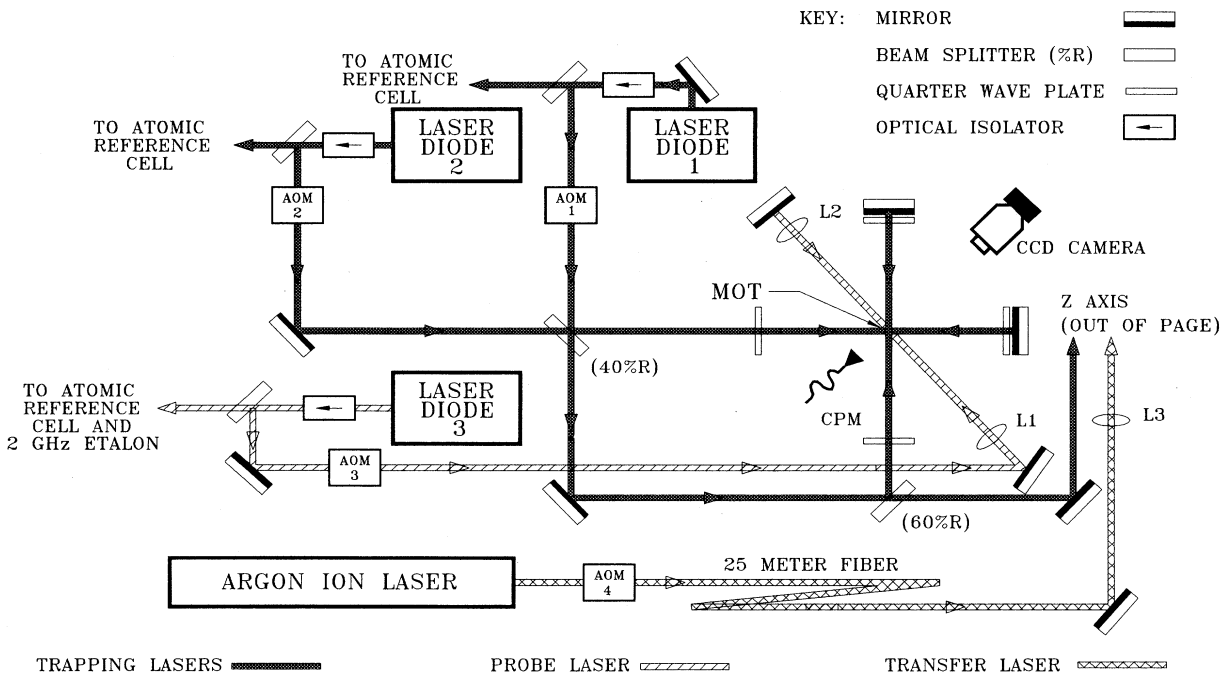

FIG. 2. Schematic of the experimental apparatus. Note that laser diode 3 focused into the MOT and retroreflected and focused using lenses $L1$ and $L2$.

ground rubidium vapor at a partial pressure of $\sim 10^{-9}$ torr. Three retroreflected laser beams intersect orthogonally at the zero-field center of a quadrupole magnetic field. A pair of coils in an anti-Helmholtz configuration produces the quadrupole magnetic field with a gradient ~ 20 G cm^{-1} through the horizontal plane. Quarter-wave plates set the appropriate polarizations, and the intensity of the $\hat{z}$ (out-of-page) beam was adjusted to one-half the intensity of the $\hat{x}$ and $\hat{y}$ beams to compensate for the stronger magnetic field gradient along the $\hat{z}$ direction. This arrangement results in a roughly isotropic confining force for the atoms, producing a near-spherical trap [7]. Two laser diodes are used to form the MOT (lasers 1 and 2 in Fig. 2), one tuned about 1 natural linewidth below the trapping transition $^2S_{1/2}(F=3) \rightarrow {}^2P_{3/2}(F'=4)$ and the other near the $^2S_{1/2}(F=2) \rightarrow {}^2P_{3/2}(F'=3)$ "repumper" transition. Total power in the trapping laser (before distribution to the three arms of the MOT) is ~ 6 mW, while power in the repumper is restricted to $\sim$ 1 mW. The trapping laser (Sharp LTO24) linewidth is narrowed to less than the atomic transition linewidth (5.9 MHz) using an external grating cavity [8], while the repumper is a free running, single mode, Sharp (LTO21) diode. Both these lasers are locked to atomic saturated absorption signals from an atomic vapor reference cell. The two laser beams are expanded to ~ 15 mm (e^{-2} point) and combined on a beam splitter (40%, where R is reflectivity, in Fig. 2) to introduce both frequencies in all arms of the MOT.

Acousto-optic modulators (AOM 1 and 2) modulate the trapping and repumper lasers at 20 kHz (50% duty cycle). When the trapping light is off, the probe laser ω_p and transfer (or ionizing) laser ω_t are switched on using AOM 3 and 4 (duty cycle slightly less than 50%). The probe laser (laser diode 3) is specified at 50 mW output power (Spectra Diode Labs SDL-5401-G1) with a bandwidth (full width at half maximum) of 15 MHz. By sweeping the drive current, we can tune roughly 2 cm^{-1} to the red and the blue of the atomic resonance. The probe laser is retroreflected and focused ($L1$ and $L2$) on the trapped atoms to get maximum intensities of $\geqslant 50$ W cm^{-2}. The transfer laser ω_t is the 476.5-nm line from an Ar^+ ion laser imported from another laboratory through an optical fiber. This beam is also focused to give 25–30 W cm^{-2} at the MOT, intersecting at an angle of 5°–10° with respect to the $\hat{z}$ axis. A charge-coupled-device camera fitted with a telephoto lens images the MOT onto a video monitor. The MOT forms typically as a near-sphere 180–220 μm in diameter. A charged particle multiplier (CPM) is mounted about 50 mm from the MOT, and a pulsed accelerating grid in front of the CPM draws ions from the MOT center. Time of flight discriminates the mass of the detected ionized species. The output from the CPM goes through a preamplifier then into a gated counter. The gated pulse counter detects and accumulates ions formed during the probe phase for 0.2–0.4 sec and gives a calibrated analog output for the number of ions detected. The probe laser is scanned at 20 MHz sec^{-1} with atomic rubidium spectral lines and 2-GHz étalon markers for frequency references. During experimental runs, an auxiliary turbomolecular vacuum pump reduces background pressures to $\sim 10^{-10}$ torr.

Sweeping the probe laser $\hbar\omega_p$ to the red of the atomic resonance (negative detuning) and counting the mass-analyzed Rb_2^+ produced generates the PAI spectrum shown in Fig. 3(a). In the detuning range from -16 to -32 GHz the spectrum is an average of 16 scans, while from -10 to -16 GHz only eight scans were included. We interpret the regularly spaced peaks as vibrational progressions in excited bound states. Stimulated PAI is a two-step process illustrated in Fig. 1(b). In the first step the probe laser couples incoming scattering flux on the ground-state hyperfine molecular curve

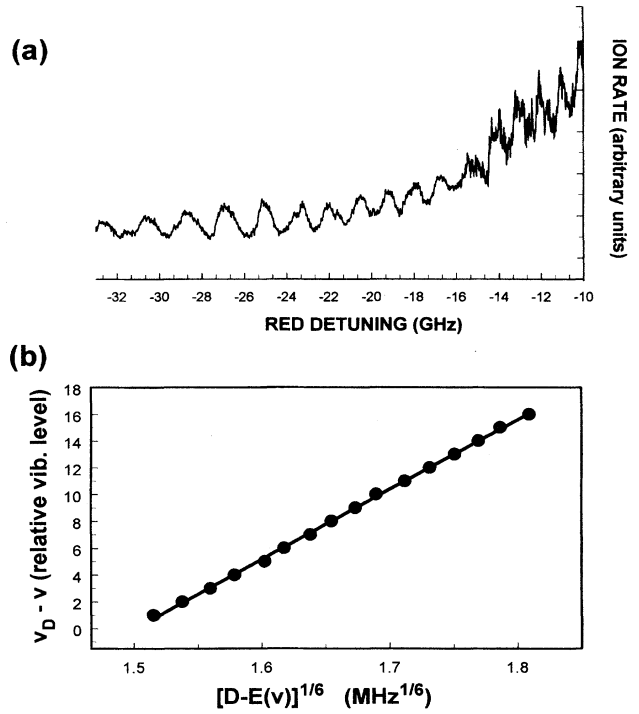

FIG. 3. (a) Measured stimulated PAI spectrum from ^{85}Rb collisions in the presence of ω_p and ω_t probe and transfer optical fields. Separation and widths of the peaks are consistent with the 1_g molecular state. (b) Plot of $v_D - v$ vs $\{[D-E(v)]/H_3\}^{1/6}$ from the data in (a). A linear regression fit yields the slope from which C_3 is determined.

labeled by the $F+F'=3+3$ asymptote to an excited attractive molecular state around the Condon point R_c where $\hbar\omega_p$ just equals the energy difference between the ground and excited molecular states, labeled by the $(F=3)+P$ asymptote. In the second step the transfer laser $\hbar\omega_t$ couples the excited molecular state to the Rb_2^+ $(^2\Sigma_g^+)+e$ ionization continuum. The transitions in the first step occur very close to the dissociation limit, where the interatomic potential has a characteristic inverse power form,

$$V(R)=D-\frac{\sum_{m\geq n} C_m}{R^m}. \tag{6}$$

The term D is the molecular dissociation limit, C_m the expansion coefficient, and n the power of the dominant term as the energy approaches dissociation. In the case of identical atoms the lowest lying bound excited molecular states are dominated by the C_3/R^3 dipole-dipole interaction at long range. LeRoy and Bernstein [9] and Stwalley [10] have shown that in this regime the spacing between vibrational levels can be described analytically by

$$\frac{dE(v)}{dv}=A_3[D-E(v)]^{5/6}, \tag{7}$$

where $E(v)$ is the energy of vibrational level v and A_3 is proportional to $C_3^{-1/3}$. Equation (7) can be integrated and rearranged to give

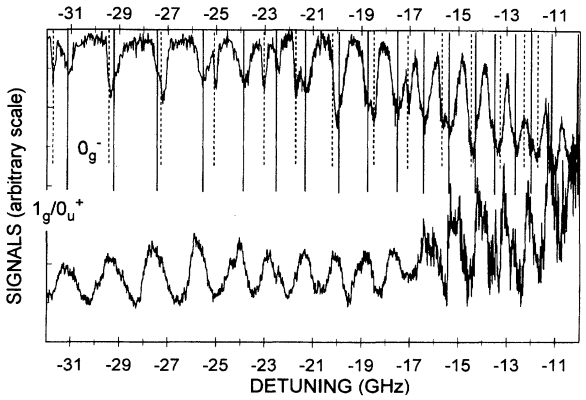

FIG. 4. Comparison of FORT spectra (top) to PAI spectra (bottom). Note the absence of 0_g^- progression in the PAI spectra.

$$v_D - v=\{[D-E(v)]/H_3\}^{1/6}, \tag{8}$$

where v_D is the effective vibrational index (integration constant). Equation (8) is used to fit the experimental data. Figure 3(b) shows the plot of (v_D-v) vs $[D-E(v)]^{1/6}$ from the slope of which we extract C_3 by standard linear regression, since

$$H_3=\hbar\left(\frac{2\pi}{\mu}\right)^{1/2}\frac{\Gamma(\frac{4}{3})}{\Gamma(\frac{5}{6})}\frac{1}{2C_3^{1/3}}. \tag{9}$$

We thus determine $C_3=(14.43\pm0.23)\,e^2a_0^2$. The quoted uncertainty is statistical and does not include systematic errors in the dissociation limit D due to molecular hyperfine effects. The regular spacing and simplicity of the spectrum suggest the presence of only one molecular state, and this measured C_3 is close to a calculated value of $14.2e^2a_0^2$ for the 1_g state, supposed accurate to within 10% [12]. It is also in good agreement with the $C_3=(14.29\pm0.02\pm0.7)e^2a_0^2$ reported for the 1_g by Cline *et al.* [11]. In this latter work the first uncertainty term is statistical and the second term estimates the systematic errors. Further support for the identification of the spectrum with the 1_g state is the fact that the 0_u^+, which has a similar C_3, predissociates at a rate about 10^6 faster than photoionization [11], and should therefore not be present in the ion spectrum. We therefore assign the PAI spectrum to the 1_g state.

Figure 4 compares the present results to those obtained from trap-loss spectra in a far-off-resonant trap (FORT) [11]. The spacing and widths of the peaks assigned to the 1_g are in reasonable accord between the PAI and trap-loss results, with noticeable differences, however, in the range -21 to -24 GHz. The width of the 1_g features in both experiments is probably due to unresolved molecular hyperfine structure [13]. The most obvious difference is the absence of the 0_g^- long-range state in the PAI spectrum. Since the initial free-bound photoassociation to the excited molecular states is quite similar in the two experiments, the explanation may be in the different probes of these states. In the FORT experiments the spectrum is generated by monitoring trap fluorescence (i.e., number of trapped atoms) as a probe laser tunes to the red of the atomic resonance transition. The spectral

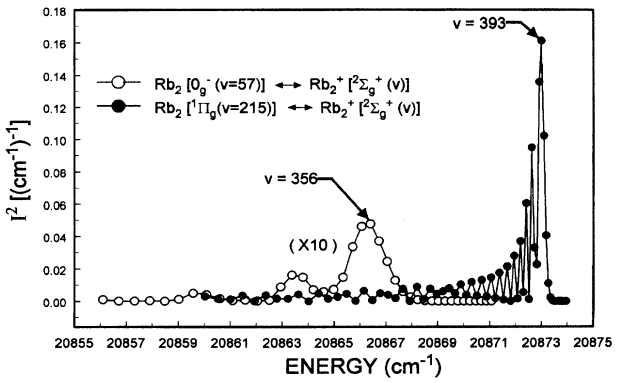

FIG. 5. Squares of the nuclear wave-function overlap integrals, I^2, plotted for $v=215$ of the 1_g and $v=57$ of the 0_g^-, over the range of vibrational levels of the molecular ion $^2\Sigma_g^+$ where I^2 attains significant amplitude. The vibrational levels $v=215$ and 57 correspond to ω_p detuning of about -25 GHz for 1_g and 0_g^-, respectively.

dips in the fluorescence are due to enhanced atom loss rate from the trap when the probe beam tunes through each resonance in the series of vibration-rotation transitions associated with the 1_g or 0_g^- states. Photoassociation of the ^{85}Rb atoms effectively removes them from the FORT. In contrast, the intensity of the PAI signal relies on a second optical coupling from the bound molecular states to the Rb_2^+ photoionization continuum. The relative probability of this second, photoionizing transition is controlled by the nuclear overlap integrals (Franck-Condon factors) between $Rb_2(1_g,0_g^-)$ and $Rb_2^+(^2\Sigma_g^+)$. Figure 5 plots I^2, the square of the overlap integral, for $0_g^-(v=57) \rightarrow {}^2\Sigma_g^+(v)$ and $1_g(v=215) \rightarrow {}^2\Sigma_g^+(v)$ over the range of final ion vibrational levels where I^2 achieves maximal value. The pure long-range 0_g^- potential was taken from Ref. [13] and the long-range part of the 1_g was splined to the $^1\Pi_g$ potential of Ref. [14]. The Rb_2^+ ion potential was taken from Spiegelmann *et al.* [15] and Krauss and Stevens [16]. The plot in Fig. 5 shows that the I^2 for 0_g^- is smaller than that for 1_g by about a factor of 20, and it is therefore not surprising that the 0_g^- does not appear in the PAI spectra.

In summary we have shown that in the ultracold regime photoassociative ionization can be generalized to systems even where the channel for conventional collisional autoionization is closed. It appears therefore that direct, two-color PAI can be added to the arsenal of spectroscopic tools available for the analysis of optically cooled and trapped species.

Financial support from the National Science Foundation, the U.S. Army Research Office, and the Office of Naval Research is gratefully acknowledged.

[1] M. Machholm, A. Giusti-Suzor, and F. H. Mies, Phys. Rev. A **50**, 5025 (1994).

[2] For a recent review of theory see P. S. Julienne, A. Smith, and K. Burnett, in *Advances in Atomic, Molecular, and Optical Physics*, edited by D. R. Bates and B. Bederson (Academic Press, San Diego, 1993), Vol. 30, p. 141.

[3] For a recent review of experiment see T. Walker and P. Feng, in *Advances in Atomic, Molecular, and Optical Physics*, edited by B. Bederson and H. Walther (Academic Press, San Diego, 1994), Vol. 34.

[4] For an update on the two earlier reviews in experiment and theory see J. Weiner, in *Advances in Atomic, Molecular, and Optical Physics* (Ref. [3]), Vol. 35.

[5] E. Raab, M. Prentiss, A. Cable, S. Chu, and D. Pritchard, Phys. Rev. Lett. **59**, 263 (1987).

[6] C. Monroe, W. Swann, H. Robinson, and C. Wieman, Phys. Rev. Lett. **65**, 1571 (1990).

[7] D. Hoffman, P. Feng, and T. Walker, J. Opt. Soc. Am. B **11**, 712 (1994).

[8] K. MacAdam, A. Steinbach, and C. Wieman, Rev. Sci. Instrum. **60**, 1098 (1992).

[9] R. J. Leroy and R. B. Bernstein, J. Chem. Phys. **52**, 3869 (1969).

[10] W. C. Stwalley, Chem. Phys. Lett. **6**, 241 (1970).

[11] R. A. Cline, J. D. Miller, and D. J. Heinzen, Phys. Rev. Lett. **73**, 632 (1994), and references cited therein.

[12] P. S. Julienne and C. J. Williams (unpublished).

[13] C. J. Williams (private communication).

[14] M. Foucrault, Ph. Millie, and J. P. Daudey, J. Chem. Phys. **96**, 1257 (1992).

[15] F. Spiegelmann, D. Pavolini, and J. P. Daudey, J. Phys. B **22**, 2465 (1989).

[16] M. Krauss and W. J. Stevens, J. Chem. Phys. **93**, 4236 (1990).